IEEE Access
Multidisciplinary | Rapid Review | Open Access Journal

Received June 26, 2020, accepted July 14, 2020, date of publication August 6, 2020, date of current version August 19, 2020.

Digital Object Identifier 10.1109/ACCESS.2020.3014814

Ultrasound Assessment of the Relation Between Local Hemodynamic Parameters and Plaque Morphology

LISHENG XU[1], (Senior Member, IEEE), YANLING ZHANG[2], LONG MENG[3], (Member, IEEE), SHUAI LI[1,4], LILI NIU[3], (Member, IEEE), STEPHEN E. GREENWALD[5], HUI ZHANG[2], AND LU WANG[6], (Member, IEEE)

[1]College of Medicine and Biological Information Engineering, Northeastern University, Shenyang 110169, China
[2]Department of Ultrasound, Third Affiliated Hospital, Sun Yat-sen University, Guangzhou 510630, China
[3]Paul C. Lauterbur Research Center for Biomedical Imaging, Shenzhen Institutes of Advanced Technology, Chinese Academy of Sciences, Shenzhen 518055, China
[4]Department of Biomedical Engineering, The Hong Kong Polytechnic University, Hong Kong
[5]Barts and The London School of Medicine and Dentistry, Blizard Institute, Queen Mary University of London, London E1 2ES, U.K.
[6]School of Computer Science and Engineering, Northeastern University, Shenyang 110169, China

Corresponding authors: Hui Zhang (zhang9@mail.sysu.edu.cn) and Lu Wang (wanglu@cse.neu.edu.cn)

This work was supported in part by the National Key Research and Development Program of China under Grant 2016YFC0104700, in part by the National Science Foundation of China (NSFC) under Grant 11574341, Grant 11774371, Grant 61773110, Grant 81701713, Grant 11674347, and Grant 61701099; in part by the Natural Science Foundation of Guangdong Province under Grant 2017B030306011, Grant 2016TQ03X716, and Grant 2016TQ03R472; in part by the Youth Innovation Promotion Association Chinese Academy of Sciences (CAS) under Grant 2018393; in part by the Fundamental Research Funds for the Central Universities under Grant N161904002; and in part by the Open Program of Neusoft Research of Intelligent Healthcare Technology, Company, Ltd., under Grant NRIHTOP1801.

ABSTRACT Mechanical factors, especially wall shear stress (WSS) and circumferential strain (CS), play an important role in the progression and rupture of atherosclerotic plaques. Previous studies have shown that the temporal phase angle between WSS and CS, referred to as the stress phase angle (SPA) may be a biomarker for plaque development and vulnerability. Since the SPA is influenced by the severity and length of the stenosis, a multifactorial relationship between local hemodynamic variables and plaque morphology can be hypothesized. However, due to ethical restrictions and the difficulty of developing animal models, there is little experimental data to support such a hypothesis about the biomarker function of SPA. In this study, a novel non-invasive ultrasound-based method for investigating the relationship between local hemodynamics and plaque morphology is developed and investigated in-vitro and in-vivo with an apolipoprotein deficient mouse model. In the in-vitro experiments, using polyvinyl alcohol cryogel (PVA-c) phantoms, we have observed that the SPA becomes more negative and the wall shear rate (WSR) rises, as the severity of the stenosis increases. Conversely, SPA becomes more positive and WSR falls with increasing plaque length. These changes in plaque morphology have little effect on CS. The in-vivo experiments show that, as the severity of the plaque increases, the SPA becomes more negative and WSR tends to more positive values; whereas, the CS drops. We conclude that these local hemodynamic parameters such as SPA, WSR and CS, as suggested by others, can be regarded as prognostic markers for the assessment of plaque vulnerability.

INDEX TERMS Local hemodynamic parameters, wall shear stress (WSS), circumferential strain (CS), stress phase angle (SPA), wall shear rate (WSR), vulnerable plaque.

I. INTRODUCTION

Cardiovascular disease (CVD) is the commonest cause of death world-wide [1]. Atherosclerosis is a major underlying cause or sequela of most CVD, including acute events such as stroke [2]. Indeed, it has been shown that acute cardiovascular events are largely due to rupture of silent, yet vulnerable, atherosclerotic plaques [3], [4]. Consequently, to detect vulnerable plaques and distinguish them from stable plaques has become increasingly important.

Arterial calcification is a powerful marker for atherosclerotic disease especially in the coronary circulation [5]. However, atherosclerosis is a highly complex disease marked by progressive endothelial injury, arterial inflammation,

The associate editor coordinating the review of this manuscript and approving it for publication was Carmelo Militello.

altered hemodynamics, and vascular remodeling, leading to plaque formation, progression and frequently rupture.

It is well known that hemodynamic forces have an important role in atherosclerosis, and, in particular at the macroscopic and cellular level, in atherogenesis [6], [7]. In 2004, Dancu *et al.* [8] found the production of NO and PGI2 (vasodilators) in bovine aortic endothelial cells, in vitro, was strongly suppressed by asynchronous hemodynamics (i.e. where WSS and CS were in anti-phase, SPA $= -180°$), when compared with synchronous hemodynamics (SPA $= 0°$); whereas the production of ET-1, a potent vasoconstrictor, was increased. At the gene expression level, quantitative competitive RT-PCR analysis showed that highly asynchronous mechanical force patterns (SPA $= 180°$) could elicit pro-atherogenic vasoactive responses in endothelial cells. Given the diverse atheroprotective effects of NO [9] and the effect of SPA on its production, it is clear that the combined effect of WSS and CS has a strong influence on the atherosclerotic process. At the clinical level, Reriani *et al.* [10] have shown that prolonged treatment with an ET-1 agonist improves coronary endothelial function, at least in patients with early atherosclerosis. Whether improving the hemodynamic environment has a similar long-term effect remains to be determined [11].

The plaque experiences two predominant forces, wall shear stress (WSS) due to blood flow and circumferential stress due to blood pressure, and these two forces have already been recognized as an effective means of predicting plaque vulnerability [12]–[15]. More than two decades ago, Qiu and Tarbell (1996) introduced a new hemodynamic parameter, which they termed the stress phase angle (SPA). It was defined as the local temporal phase angle between the dynamic CS and WSS. In a numerical simulation of flow through anastomoses, they observed a large difference in the SPA between the proximal and distal ends of their models [16]. In a later study, they also mimicked pulsatile flow in a curved tube model of a coronary artery and demonstrated that the SPA was more negative than in other straight vessels [17]. Based on these observations, they proposed that the SPA probably played an essential role in the remodeling of the vessel wall and the development of atherosclerosis. Dalin Tang, *et al.* pointed out that computational mechanical analysis had the potential to improve accuracy in the assessment of plaque vulnerability [18]. In 2005, Tada and Tarbell published a simulation study of a carotid bifurcation to observe the relationship between the SPA and plaque occurrence and found that the location of the plaque was frequently associated with regions of large negative SPA [19]. Two years later, Tada *et al.* (2007) provided a theoretical model to examine the effect of the SPA by using the strain energy density of the endothelial cell plasma membrane. Their study showed a significant role of the SPA at the upstream and downstream ends of the cell, which are the regions where mechano-transduction is likely to occur [20]. Meanwhile, studies with stenosis models proved that the SPA could be a crucial indicator of plaque vulnerability [21], [22]. In Sadeghi's study [22], physical and computational models were used to better understand the effects of increasing stenosis severity on hemodynamics, specifically to assess the correlation between SPA and WSS. It was found that an increase in stenosis severity is associated with higher WSS and larger negative SPA, and the subsequent increasing complexity of hemodynamic patterns affects the correlation between WSS and SPA such that at low WSS the correlation is strong. However, when WSS > 1, this was not the case. The study also investigated the correlation between the low mean WSS, high oscillatory shear index and the large negative SPA at the distal shoulder and post-stenotic areas.

In 2012, Belzacq *et al.* presented a numerical parametric study of the mechanical interaction of pulsatile blood flow with axisymmetrically stenosed arteries [23]. The effect of changes in stenosis length and severity were investigated. Lengths varied from 5 mm to 20 mm (in 5 mm steps), and the severities varied from 20% to 70% (20%, 35%, 45%, 55% and 70%). They observed different types of shear stress distribution in the fibrous, corresponding to different lengths and severities of stenosis. They found that the stress distribution was dependent on stenosis length (L) and severity. Whereas long plaques (L $>= 10$ *mm*) are mostly deformed under the action of blood pressure, it appeared that shorter plaques (L < 10 *mm*) were significantly affected by the shear stresses. Specifically, high stresses were localized to the upstream of stenoses of moderate severity and length $>= 10$ *mm*; whereas in shorter lesions they tended to occur downstream. It was suggested that shear stresses might distort the plaque by squeezing it, thus causing the lumen of the affected artery to become narrower. This phenomenon was termed "the pinching effect". These findings offer some new perspectives for the detection of plaque vulnerability [23]. However, only computational simulations were used in these studies, so for further verification, a reliable method to measure WSS and CS simultaneously is needed to facilitate the study of the relationship between the SPA and other hemodynamic variables.

In the last fifteen years, several techniques have been developed to measure both vessel motion and blood flow velocity. For instance, Wise *et al.* (2005) measured blood flow velocity in mouse hearts from phase contrast cine MRI images [24]. Later, an MRI technique was described by Sampath *et al.* (2008) in which myocardial motion and ventricular blood flow were measured both in healthy humans and pigs with mitral regurgitation [25]. However, for MRI the low temporal resolution is a critical limitation, resulting in the need for long-duration imaging sequences. These temporal constraints do not apply to intravascular ultrasound (IVUS) and a number of such studies on patients suffering from cardiovascular disease have been published. Ge *et al.* (1999) screened ruptured plaques in patients with coronary artery disease by intravascular ultrasound [26] and in 2000, Yamagishi *et al.* studied the morphology of vulnerable coronary plaques using the same technique [27]. At this time a clinical expert consensus document on standards for acquisition, measurement and reporting on IVUS was published [28]. In this document, morphological descriptors of

atheromata such as the length of stenosis, calcium content, plaque echo-lucency, degree of fibrosis, thrombus, intimal hyperplasia and so on, were listed. Any combination of these factors might be used as a diagnostic standard. Beulen *et al.* developed a new cross correlation-based method for measuring local pressure waveforms in large arteries by using ultrasound [29]. The pressure values were predicted with a precision of 1.5 *mmHg*, demonstrating that a noninvasive pressure assessment in large arteries by means of ultrasound is feasible [29]. Furthermore, Sethuraman *et al.* (2008) showed that the different components of atherosclerotic plaques could be identified with spectroscopic intravascular photo-acoustic imaging [30]. And several studies have provided histological evidence that the volume of the individual components in an atherosclerotic plaque can be determined with ultrasound on the basis of the image texture and wave speed of the various materials within the plaque [31], [32]. However, IVUS is invasive and thus not recommended for superficial arteries such as the carotid, because duplex ultrasound, which is non-invasive, can be used instead. Hence, a non-invasive ultrasonic method that can measure the arterial wall displacement and blood flow pattern simultaneously with ultrasonic B-mode contrast images has been developed [33]. This method is particularly suitable for estimating vessel diameter and blood flow velocity and then for calculating local derived hemodynamic parameters. Here, it is applied to measure WSS, CS and SPA both in vitro and in vivo. With this technique, we wish to determine accurately the relationship between these hemodynamic parameters and, in future work, hope to use the technique in clinical studies of patients with a variety of cardiovascular pathologies. Our aim is to assess the relationship between these local hemodynamic parameters and the size and severity of the plaque by carrying out measurements in-vitro and in-vivo, with an apolipoprotein deficient mouse model.

II. METHODS

A. LOCAL HEMODYNAMIC PARAMETERS

WSS results from the shearing force of blood flow, CS is a cyclic strain driven by the pressure wave, and SPA ($\Delta\varphi_s\,(\gamma_c, \tau_w)$) is defined as the temporal phase angle between CS (γ_c) and WSS (τ_w) [34].

$$\tau_{\mathrm{w}}\,(\mathrm{t}) = \mu\frac{\partial \mathrm{v}\,(\mathrm{t})}{\partial \mathrm{n}} \tag{1}$$

$$\gamma_{\mathrm{c}}(\mathrm{t}) = \mathrm{D}(\mathrm{t})/\mathrm{D}_{\mathrm{mean}} \tag{2}$$

$$\Delta\varphi_{\mathrm{s}}\,(\gamma_{\mathrm{c}}, \tau_{\mathrm{w}}) = \varphi\,(\gamma_{\mathrm{c}}) - \varphi(\tau_{\mathrm{w}}) \tag{3}$$

where μ is dynamic viscosity of the fluid, $\frac{\partial v}{\partial n}$ denotes the gradient of the tangential velocity in a direction normal to the wall, D is the diameter of the vessel and φ, the phase angle between circumferential strain and wall shear stress. To be more specific, in equation 2, D_{mean} is the average of D_{max} and D_{min} which are the diameters measured at the end of systole and diastole, respectively. Given the difficulty of measuring arterial CS directly, it is represented by the variation of arterial diameter, on the basis that it is almost synchronous with the change of transmural pressure [35]. Thus, equation 3 can be replaced by

$$\Delta\varphi_s = \varphi\,(D(t)) - \varphi(\tau_w) \tag{4}$$

Blood flow velocity can be measured ultrasonically. Since the WSS is defined as the viscosity (μ = constant) times the wall shear rate (WSR), the phase of the WSS can be replaced by the phase of the WSR, i.e.:

$$\Delta\varphi_{\mathrm{s}} = \varphi\,(\mathrm{D(t)}) - \varphi(\dot{\gamma}_{\mathrm{w}}) \tag{5}$$

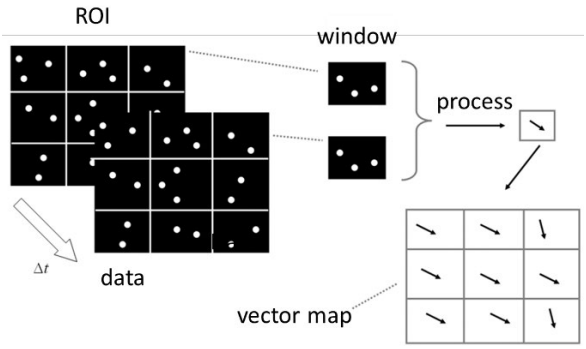

FIGURE 1. Schematic diagram of PIV processing.

B. ULTRASONIC MEASUREMENT TECHNIQUES

To determine $\Delta\varphi_{\mathrm{s}}$, two measurements must be performed, namely the displacement of the vessel wall and the velocity of blood flow. In this study, the ultrasonic method proposed by Niu *et al.* was used [36]. Briefly, microbubbles were injected into the flow and the flow field was determined by echo particle image velocimetry (EPIV), using a sampling frequency of 175 *Hz*. Fig. 1 summarizes the process. The diameter of each particle was between 1 and 5 μm, the interrogation window size was around 200×90 pixels and the percentage of window overlap was 50%. For the PIV calculation, we used the algorithms in references [36], [37]. Their performance was assessed by analyzing simulated images with known displacements, and ultrasonic B-mode images of in vitro laminar pipe flow, rotational flow and in vivo rat carotid arterial flow [36]. For laminar flow, the new algorithm gave a 1.1% deviation from the analytically derived value. The vector quality evaluation for the rotational flow imaging showed that this algorithm could produce much smaller bias from the known velocity vectors. For in vivo rat carotid arterial flow imaging, the results from the new algorithm deviated by an average of 6.6% from the Doppler-measured peak velocities, compared to 15% from those of the conventional algorithm. Therefore, we conclude that the Echo PIV algorithm is able to effectively improve the measurement accuracy in imaging flow fields with high velocity gradients.

For each frame captured by the ultrasound system, a region of interest (ROI) was selected and then the ROI was divided into nine windows, from which a vector map was drawn, as shown in Figure 1. The CS can be calculated from the displacement of the arterial wall, and the WSR can be estimated from the gradient of the local flow velocity.

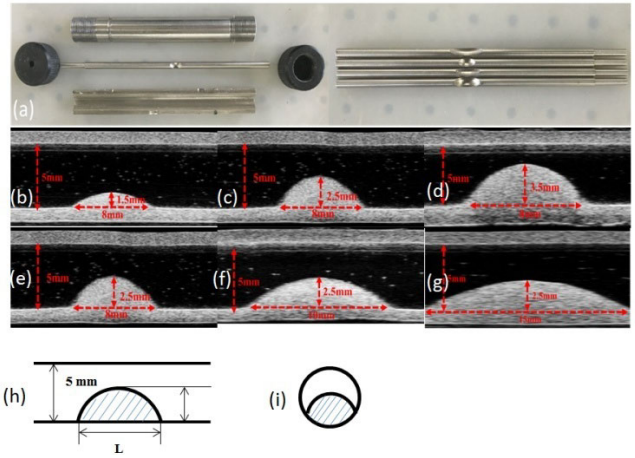

FIGURE 2. (a) The components of the phantom-molds. (b)-(d), three stenoses with fixed length of 8 mm and diameter ratios of 30%, 50%, and 70%, respectively. (e)-(g), three stenoses of length of 8 mm, 10 mm and 15 mm with a fixed 50% severity. (h)-(i), longitudinal and cross-sectional view of the stenosed artery.

C. STATISTICAL ANALYSIS

To assess the significance of the relationship between the haemodynamic variables and those describing the plaque morphology, one-way ANOVA was used. Statistical significance was specified by a p value <0.05.

D. EXPERIMENTAL SET-UP: POLYVINYL ALCOHOL (PVA) ARTERIAL PHANTOM IN VITRO

PVA cryogel, a water-soluble synthetic polymer derived from the hydrolysis of polyvinyl acetate was used as the phantom soft tissue-mimicking material because of its acoustic and physical properties. The mechanical properties of PVA can be modified by repeated freeze-thaw cycles, such that it becomes stiffer with each cycle. The elasticity of the phantom is also affected by the PVA/water ratio. King *et al.* (2011) reported that in a 10% PVA cryogel vessel phantom made with five freeze-thaw cycles, the speed of sound and Young's modulus were 1550 m/s and 160 kPa, respectively [38]. In the work of Fromageau *et al.* (2003), the PVA cryogel solution was also composed of 10% polyvinyl alcohol dissolved in water, but powdered silica (1% by weight) was added to enhance U/S scattering during the initial preparation of the gel [39].

In the current study, the PVA vessel phantom consisted of (by weight) 87% de-ionized water, 10% PVA powder (SIGMA-ALDRICH) and 3% silica powder (SIGMA-ALDRICH). After being agitated at 100 rpm and 95°C for 1h, the viscous mixture was put in an ultrasonic cleaner (Shenzhen Mengjie Ultrasonic Cleaner Ltd, mini-size) for a minimum of 15 minutes to ensure no air bubbles remained. Then the mixture was poured into a metal mold at room temperature. All molds consisted of four common parts (Fig. 2(a)-left): top-cap, bottom-cap, solid rod with diameter of 5 mm (to simulate the inner diameter of the artery), and shell with diameter of 7 mm. Thus, in this case, the wall thickness of the arterial phantom was fixed at 1 mm, and the outer diameter of the arterial phantom, at 7 mm. The only difference in the models was the shape of the depression on the rod, as shown in Fig. 2(a)-right, so that specifically shaped plaques could be created within the vessels. All phantoms were prepared using seven sequential freeze-thaw cycles, each cycle consisting of 12h freezing at −20°C and 12h thawing in water at around 20°C. After that, the top-cap and bottom-cap could be pulled apart, and the solid rod then removed from both ends without damaging the stenosis, leaving the phantom with a stenotic plaque. One group of phantoms each contained a single stenotic plaque of diameter ratio 30%, 50%, or 70% (fixed length of 8 mm), as shown in Figs. 2(b)-(d). A second group comprised three PVA-c phantoms with plaques of different lengths, i.e 8 mm, 10 mm and 15 mm, with the same diameter ratio (50%), as shown in Figs. 2(e)-(g). All the plaques are spherical segments. Figs. 2 (h)-(i) are longitudinal and cross-sectional views of the stenosed arteries.

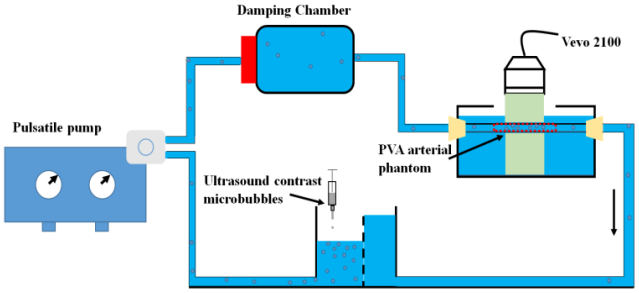

FIGURE 3. Schematic overview of the in-vitro experimental set-up. The micro-bubbles are injected into the partitioned tank by a 1 mL syringe, and for the volume of the whole system and the concentration of the microbubble solution, one drop was sufficient for visualization.

E. EXPERIMENTAL PERFUSION SYSTEM

To simulate the blood circulation, a perfusion system was built, as shown in Fig. 3. A pulsatile pump (Model 55-3305; Harvard Apparatus, Holliston, MA, USA) was used to generate pulsatile flow (at a rate of 40 beats/min). De-ionized water was pumped through a damping chamber, to avoid over-expansion of the phantom and thence through the PVA arterial phantom immersed in a water tank. Degassed water was used to avoid image degradation by ultrasound scattering from air bubbles. In the imaging section, a scanning ultrasound probe (MS250, frequency 21 MHz), was positioned parallel to the long axis of the artery, centered over the point of maximum lumen reduction, perpendicular to the outer surface of the stenosis and connected to an ultrasound imaging system (Vevo 2100, Visual Sonics, Toronto, ON, Canada). A sequence of 2D ultrasound B-mode images was acquired at a frame rate of 175 Hz. To assess the flow velocity with echo PIV, ultrasound contrast micro-bubbles at a concentration of 5.0×10^8 micro-bubbles ml^{-1} were used as the scattering medium [40]. The Reynolds number of the de-ionized water with micro-bubbles is 15.93, therefore, the blood flow in the artery phantom is assumed to be laminar.

F. IN-VIVO EXPERIMENT: MODEL ESTABLISHMENT

Twenty apolipoprotein E-deficient (ApoE-/-) mice aged five to six-weeks were purchased from Vital River Laboratory

Animal Technology Co. Ltd. (Beijing, China). All procedures were approved by the Medical Ethical Committee of The Shenzhen Institutes of Advanced Technology. A stenosis model was established by feeding the animals a hypercholesterolemic diet (HCD, containing 21% fat and 0.15% cholesterol by weight) for almost 10 months [9]. After that, the mice were divided into two groups based on the plaque's size, one group with a severity $< 50\%$ and the other with a severity $> 50\%$. All plaques were assessed by a cardiologist, specialized in ultrasonic diagnosis. During this process, not all mice presented with a clearly defined plaque in their common carotid arteries (CCA). Furthermore, some mice died unexpectedly during the experiment. The cause of death is not only due to old age (10 months), but also the blood volume of mice is less. If more microbubbles are injected, the effective ejection volume of mice will be insufficient, and the mice will die due to heart failure. As a result, only four mice from each group were measured.

G. IN-VIVO EXPERIMENTAL PROTOCOL

Mice were anesthetized with isoflurane gas at a dose of 1% in pure oxygen and a flow rate of 1 $L\ min^{-1}$. The necks were shaved to ensure that the fur would have no effect on image quality. Body temperature was maintained close to 36.2°C by a heating pad. The left CCA was imaged by the same Vevo 2100 system (and MS250) as used in the in-vitro experiments. The frame rate was 175 Hz. Ultrasound contrast microbubbles (concentration $2.0 \times 10^5 ml^{-1}$ in 0.1 ml saline) were injected via a tail vein, as the tracker. After the animal experiments were completed, the mice were perfused with 0.9% saline and then underwent perfusion fixation with 4% paraformaldehyde introduced to the left ventricle through the apex of the heart. The left common carotid arteries were excised and fixed in 4% paraformaldehyde for 48 hours. Finally, serial cryosections of 6 μm thickness were cut and stained with hematoxylin and eosin (H&E) to confirm plaque morphology.

III. RESULTS

A. IN VITRO

In this study, we have focused primarily on the WSS (WSR) around the stenosis. Although, deformation of the plaque is expected to occur [23], [41], our calculations showed that the deformation due to the blood flow and the movement of the arterial wall were small. Experimentally, we did not observe any deformation of the plaque and since the resolution of the Vevo® 2100 is 30 μm, we conclude that the deformation was less than this. Thus, we did not account for the effect of plaque deformation when calculating WSS and CS, focusing instead on the WSS (WSR) around the stenosis.

The results from the three constant length phantoms with 30%, 50% and 70% diameter reduction are shown in Figs. 4, 5 and 6, respectively. Some details of the related algorithm are described in [36]. The corresponding WSR, CS and the SPA are shown in subfigure (a). In subfigure (b), the upper panel is the US image and the lower panel indicates the spatial

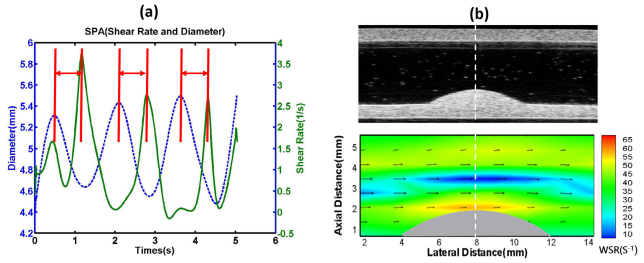

FIGURE 4. Results for the phantoms with fixed length of 8 mm and stenosis severity of 30%. (a) WSR, CS and the SPA. (b) Upper panel is the US image and the lower panel indicates the spatial distribution of flow velocity and WSR. (Data for three pump cycles.)

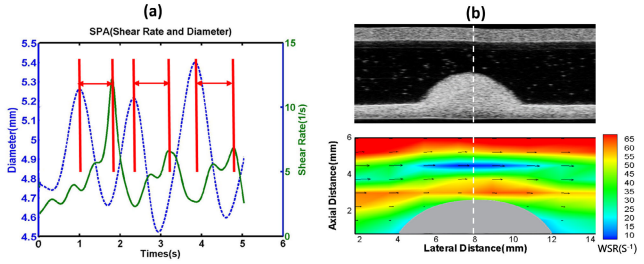

FIGURE 5. Results for the phantoms with fixed length of 8 mm and stenosis severity of 50%. (a) WSR, CS and the SPA. (b) Upper panel is the US image and the lower panel indicates the spatial distribution of flow velocity and WSR. (Data for three pump cycles.)

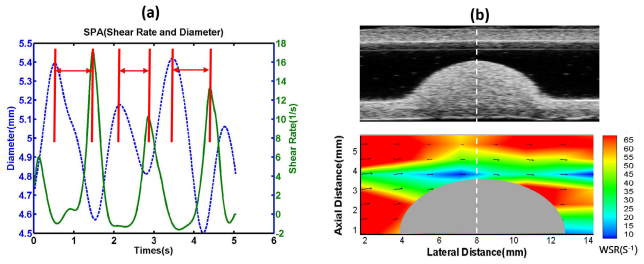

FIGURE 6. Results for the phantoms with fixed length of 8 mm and stenosis severity of 70%. (a) WSR, CS and the SPA. (b) Upper panel is the US image and the lower panel indicates the spatial distribution of flow velocity and WSR. (Data for three pump cycles.)

distribution of flow velocity and WSR. The WSR, and CS shown in subfigure (a) are corresponding to the narrowest position along the white dash line in subfigure (b). As mentioned above, the resolution of the ultrasound scanner used for the arterial phantom measurements (Vevo® 2100), is about 30 μm. Thus, in this study, more highly-resolved velocity fields cannot be observed, unless the window size is reduced. If the resolution is increased beyond this, the window size becomes too small to observe enough cycles. We need to acquire at least two or three cycles which implies that, currently, the US imaging device cannot achieve the accuracy of an optical device. However, current optical devices are invasive whereas our ultrasound approach is not.

With increasing plaque severity, the WSR and hence WSS increased. The panels in the middle row of Figs, 4-6 show, for each stenosis severity, the variation with time of diameter (blue dashed line) and WSR (green) at the narrowest position of the arterial phantom. The vertical red lines indicate the

TABLE 1. Mean values ± standard deviations of SPA, WSR and CS for different stenosis severities.

Stenosis severity	30%	50%	70%	p
SPA (°)	177.46±11.72	207.50±10.90	227.68±21.54	0.020
WSR (1/s)	3.32±0.45	9.59±4.50	13.81±3.19	0.019
CS (%)	8.22±1.86	7.85±2.59	6.42±3.03	0.674

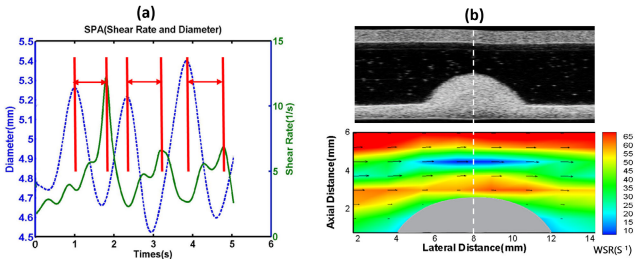

FIGURE 7. Results for the phantoms with stenosis severity of 50% and length 8 mm. (a) WSR, CS and the SPA. (b) Upper panel is the US image and the lower panel indicates the spatial distribution of flow velocity and WSR. (Data for three pump cycles.)

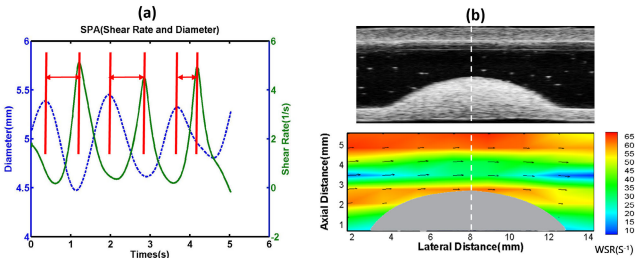

FIGURE 8. Results for the phantoms with stenosis severity of 50% and length 10 mm. (a) WSR, CS and the SPA. (b) Upper panel is the US image and the lower panel indicates the spatial distribution of flow velocity and WSR. (Data for three pump cycles.)

local maxima of the diameter and WSS signals. The SPA is then derived from the time difference between each pair of maxima as shown by the horizontal arrowed lines. Note that data are shown for three pump cycles. In addition, the spatial distribution of flow velocity is shown in the bottom row where higher velocity implies a greater WSS. In this study, all the WSRs are shown at the moment when blood flow was maximal and thus exposing the plaque to maximal wall shear stress or rate.

The relationships between the hemodynamic parameters and stenosis severity are listed in Table 1, which supports previous findings that plaque stability is associated with WSS [12]–[14], demonstrating that SPA and WSR increase significantly with increasing stenosis severity ($p = 0.02$ and 0.019 respectively, one-way ANOVA). On the other hand, the CS decreases with increasing diameter ratio, although this association was not statistically significant, presumably because the stiffness of all three phantoms was similar, having been made from the same PVA gel subjected to the same number of freeze/thaw cycles.

The results from the three constant diameter ratio phantoms with length 8, 10 and 15 *mm* are shown in Figs. 7, 8 and 9, respectively. Figs. 7(a), 8(a), 9(a), show the variation with time of diameter (blue line), WSR in green

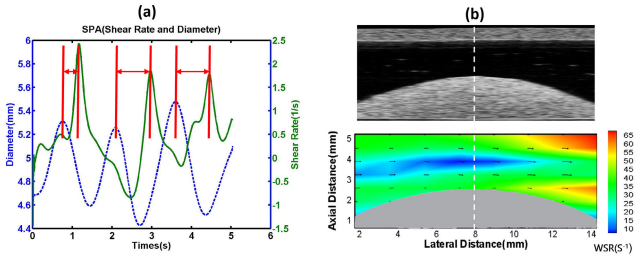

FIGURE 9. Results for the phantoms with stenosis severity of 50% and length 15 mm. (a) WSR, CS and the SPA. (b) Upper panel is the US image and the lower panel indicates the spatial distribution of flow velocity and WSR. (Data for three pump cycles.)

TABLE 2. Mean values ± standard deviation (data for three pump cycles) of SPA, WSR and CS for different stenosis lengths.

The length of the stenosis	8 *mm*	10 *mm*	15 *mm*	p
SPA (°)	207.50±10.90	182.59±32.28	-174.98±2.57	0.464
WSR (1/s)	9.59±4.50	4.60±0.40	2.023±0.35	0.032
CS (%)	7.85±2.59	7.35±1.22	6.98±2.31	0.882

and SPA, horizontal red lines. The mean values of each variable are listed in Table 2. For SPA and CS, the effect of different stenosis lengths was less pronounced than that due to the severity, ($p = 0.464$ and $p = 0.882$, respectively). However, the strongly decreasing value of WSR with increasing stenosis length is notable and statistically significant, ($p = 0.032$). The negative correlation between WSR and length implies that shorter stenoses cause more flow disturbance, a result in keeping with the simulations of Belzacq *et al.* [23]. This is implied by the WSR distribution (lower panels) too. In addition to CS, longitudinal stretch is also of importance when studying the effect of mechanical factors in atherogenesis [41]. In this study, the phantom was assumed to be isotropic. CS is represented by the variation of arterial diameter, on the basis that it is almost synchronous with the change of transmural pressure [36]. Given the assumption of isotropy, the variation of longitudinal stretch and the variation of CS would also be synchronous. Here, the SPA is the phase difference between CS and WSR. The influence of longitudinal stretch will be investigated in future work.

B. IN VIVO

Figs. 10 and 11 show the variation of diameter and WSR profiles with time for the four mice in the small plaque group and the other four in the large plaque group, respectively. Animals were assigned to either group on the basis of stenosis severity (greater or less than 50% diameter stenosis) as assessed by a clinician with extensive experience of vascular ultrasonic diagnosis. As before, the blue dashed line denotes the diameter, the green curve shows the shear rate and the phase angle differences are marked by the red lines. Typical tissue sections, having been stained with Hematoxylin-Eosin (HE), are depicted at the right and demonstrate the size of the plaques in the CCA. The values of the hemodynamic

TABLE 3. SPA, WSR and CS in both small and large plaque groups. Values for each animal (1-4) are shown with mean and standard deviation (SD) for each group. *P* value indicates the significance of difference between the two groups.

	Small plaque group					Large plaque group					*p*
	1	2	3	4	Mean ± SD	1	2	3	4	Mean ± SD	
SPA (°)	-146.25	-175.14	-130.00	-130.91	-145.57±21.07	-246.86	-240.00	-220.35	-216.13	-230.84±14.91	0.001
WSR (1/s)	2.07	0.30	0.62	1.56	1.13±0.82	1.48	5.51	5.00	1.29	3.32±2.25	0.080
CS (%)	15.17	18.81	20.79	15.10	17.47± 2.81	3.38	9.42	14.02	9.69	9.13±4.37	0.018

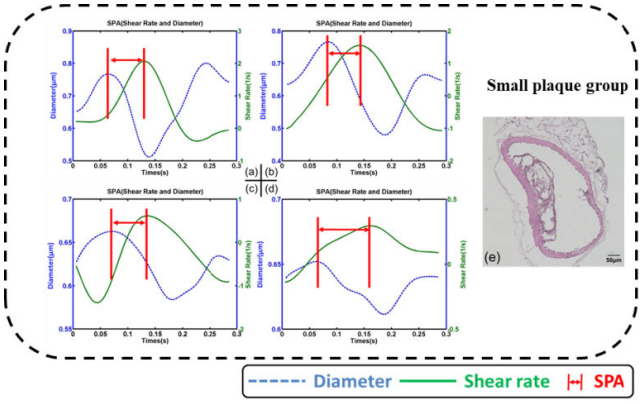

FIGURE 10. Variation of diameter, shear rate and shear phase angle in the common carotid artery of the small plaque group. (Data for one cardiac cycle.) Results for each of the four animals are shown in (a)-(d). Representative plaque cross sections are seen in (e). Hematoxylin-Eosin (HE)-stained CCA section.

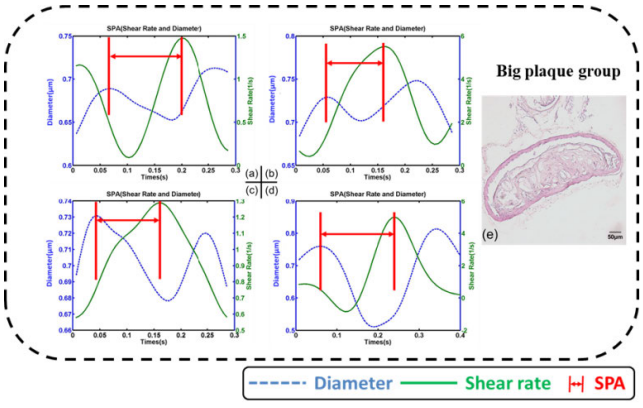

FIGURE 11. Variation of diameter, shear rate and shear phase angle in the common carotid artery of the large plaque group. (Data for one cardiac cycle.) Results for each of the four animals are shown in (a)-(d). Representative plaque cross sections are seen in (e). Hematoxylin-Eosin (HE)-stained CCA section.

variables in both groups are listed in Table 3. One-way ANOVA shows that SPA was significantly greater in the large plaque group when compared to the small plaque group. Mean CS was also increased although this difference was not significant at the 5% level. In contrast to the in-vitro experiments there is also a significant association ($p = 0.018$) between CS and plaque severity such that circumferential strain was reduced in the large plaque group.

IV. DISCUSSION

In this study we have investigated the relationship between plaque morphology and hemodynamic variables by using ultrasound. The phantom experiments reveal that, as plaque severity increases, SPA attains a larger absolute value while WSR increases and CS is reduced. On the other hand, as plaque length increases (and severity remains constant) the opposite trend is seen. The animal experiments support these findings regarding degree of stenosis (as judged by an expert in ultrasound imaging), although the plaque length was not measured. These experimental results agree with the findings of Qiu and Tarbell (2007) [17], Tada and Tarbell [19], Tada *et al.* [20], and those of Sadeghi *et al.* [22]. They are also consistent with Belzacq's numerical results [23]. It was found that an increase in stenosis severity (diameter ratio) is associated with higher WSS and a larger negative SPA. Before trying our assessment on patients, our intention was to establish an experimental animal model, such as the mouse, and to find out whether this relationship exists or not. Gratifyingly, we detected the same phenomenon in mice (cardiac cycle approximately 0.2s). In a future study, we intend, subject to ethical approval, to try it on patients.

In addition, one of the main reasons for undertaking this study was to investigate the effectiveness of the ultrasonic measurements. This is illustrated in Fig. 12 which shows vortex velocity profiles downstream of the stenosis with 30%, 50% and 70% plaque. When the stenosis severity increases, the velocity grows, and the vorticity becomes more pronounced.

This work supports the view that hemodynamic variables are becoming more widely accepted as a prognostic tool for predicting potentially vulnerable plaques. However, as most of the work on this topic has been based on fluid-structure interaction simulations, there remains a need for in-vivo studies to test the effectiveness of such a prognostic approach.

This study has some experimental limitations which need to be addressed in future work. First, the pulsatile flow rate of 40 beats/min is not representative of the typical human heart rate of around 70. We acknowledge this disparity and that neither of these rates are comparable with that of the mouse (heart interval 0.2s, corresponding to a heart rate of 300 beats/min). The phantom used in the in-vitro experiments is extremely fragile and is more easily damaged at higher heart rates, due to the increased mean pressure in

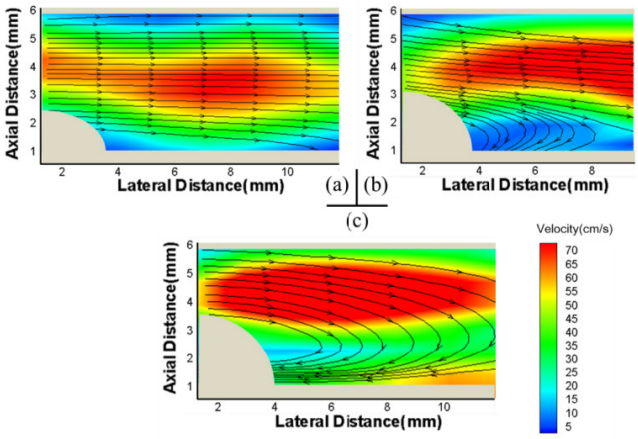

FIGURE 12. Vorticity profiles downstream from stenoses with different severities, (a) 30%, (b) 50%, (c) 70%.

the perfusion system. Previous experience had shown that 40 bpm was a feasible maximum, so we chose this as the closest approximation to a realistic human heart rate we could reasonably achieve [42]. In future, a layered arterial phantom will be developed for the in-vitro experiment, and the effect of different heart rates will to be investigated, to properly illustrate the influence of heart rate. Second, due to the limited video length of the Vevo 2100, the maximum recording duration that could be achieved in the phantom experiments was 3 cycles. The lower number of cycles in the in-vivo study was due to the higher imaging resolution needed in this experiment. The spatial resolution of the ultrasound scanner limited the accuracy with which velocity could be measured, especially near the stenosis. In principle, higher resolution can be achieved if the window size is reduced. However, it then becomes too small to observe enough cycles and it is better to acquire at least two or three cycles. This implies that, currently, the US imaging device cannot achieve the accuracy of an optical device. However, the advantage of using our US technique is that it has a large penetration depth and is non-invasive. To achieve higher resolution in the animal study, we recorded fewer cycles but repeated the measurements 3 times to obtain an average value. Third, in atherosclerotic arteries, longitudinal stretch may also be as important as CS. However, as the motivation of this study was to assess the relationship between these local hemodynamic parameters (WSS, CS and SPA) and the size and severity of the plaque through in-vitro and in-vivo studies, we chose not to investigate the effect of longitudinal stretch here. In future work, we plan to measure and investigate the effects of this variable.

V. CONCLUSION

To sum up: in the in-vitro experiments, SPA becomes increasingly negative and WSS rises with increasing stenosis severity, while the converse is seen as the length of the stenosis increases. However, for all stenosis dimensions, the CS changes little, presumably because all the PVA arterial phantoms have a similar stiffness. For the animal experiments, as for the phantoms, increasing plaque size is associated with increased WSR and more negative values of SPA. Many previous studies have regarded WSS or CS as indicators of plaque vulnerability. However, in keeping with others which provide evidence that SPA is a marker of plaque vulnerability [21], [22], this study adds weight to that evidence and supports the idea that ultrasonic detection of plaques and analysis of the associated flow disturbances is a valuable prognostic technique with many advantages over the more invasive methods currently in use. The next step is to extend the measurements to patients with occlusive vascular disease in whom the vulnerability of various types of plaque in susceptible arteries and the measurement of their mechanical properties can be detected or predicted using this non-invasive ultrasonic biomechanical approach.

ACKNOWLEDGMENT

(Lisheng Xu and Yanling Zhang are co-first authors.)

REFERENCES

[1] J. B. Emelia, J. B. Michael, and S. Chiuve, "Heart disease and stroke statistics—2017 update: A report from the American heart association," *Circulation*, vol. 135, no. 10, pp. e146–e603, 2017.
[2] G. S. Getz and C. A. Reardon, "Use of mouse models in atherosclerosis research," in *Methods in Mouse Atherosclerosis*, vol. 1339. New York, NY, USA: Humana Press, 2015, pp. 1–16, doi: 10.1007/978-1-4939-2929-0_1.
[3] C. Palombo and M. Kozakova, "Arterial stiffness, atherosclerosis and cardiovascular risk: Pathophysiologic mechanisms and emerging clinical indications," *Vascular Pharmacol.*, vol. 77, pp. 1–7, Feb. 2016.
[4] P. Eshtehardi and Z. Teng, "Protective or destructive: High wall shear stress and atherosclerosis," *Atherosclerosis*, vol. 251, pp. 501–503, Aug. 2016.
[5] J. B. Emelia, S. V. Salim, and W. Clifton, "Heart disease and stroke statistics—2018 update: A report from the American heart association," *Circulation*, vol. 137, no. 12, pp. e67–e492, Mar. 2018, doi: 10.1161/CIR.0000000000000558.
[6] H. M. Honda, T. Hsiai, and C. M. Wortham, "A complex flow pattern of low shear stress and flow reversal promotes monocyte binding to endothelial cells," *Atherosclerosis*, vol. 158, no. 2, pp. 385–390, Oct. 2001.
[7] Y. S. Chatzizisis, M. Jonas, and A. U. Coskun, "Prediction of the localization of high-risk coronary atherosclerotic plaques on the basis of low endothelial shear stress: An intravascular ultrasound and histopathology natural history study," *Circulation*, vol. 117, no. 8, p. 993, 2008.
[8] M. B. Dancu, D. E. Berardi, and J. P. V. Heuvel, "Asynchronous shear stress and circumferential strain reduces endothelial NO synthase and cyclooxygenase-2 but induces endothelin-1 gene expression in endothelial cells," *Arteriosclerosis Thrombosis Vascular Biol.*, vol. 24, no. 11, pp. 2088–2094, 2004.
[9] K. Tanaka, M. Sata, D. Fukuda, Y. Suematsu, N. Motomura, S. Takamoto, Y. Hirata, and R. Nagai, "Age-associated aortic stenosis in apolipoprotein E-deficient mice," *J. Amer. College Cardiol.*, vol. 46, no. 1, pp. 134–141, Jul. 2005.
[10] M. Reriani, E. Raichlin, and A. Prasad, "Long-term administration of endothelin receptor antagonist improves coronary endothelial function in patients with early atherosclerosis," *Circulation*, vol. 122, no. 10, p. 958, 2010.
[11] U. Förstermann and W. C. Sessa, "Nitric oxide synthases: Regulation and function," *Eur. Heart J.*, vol. 33, no. 7, pp. 829–837, 2012.
[12] E. Cecchi, C. Giglioli, S. Valente, C. Lazzeri, G. F. Gensini, R. Abbate, and L. Mannini, "Role of hemodynamic shear stress in cardiovascular disease," *Atherosclerosis*, vol. 214, no. 2, pp. 249–256, Feb. 2011.
[13] B. R. Kwak, M. Bäck, M.-L. Bochaton-Piallat, G. Caligiuri, M. J. A. P. Daemen, P. F. Davies, I. E. Hoefer, P. Holvoet, H. Jo, R. Krams, S. Lehoux, C. Monaco, S. Steffens, R. Virmani, C. Weber, J. J. Wentzel, and P. C. Evans, "Biomechanical factors in atherosclerosis: Mechanisms and clinical implications," *Eur. Heart J.*, vol. 35, no. 43, pp. 3013–3020, Nov. 2014.

[14] Y. S. Chatzizisis, A. P. Antoniadis, J. J. Wentzel, and G. D. Giannoglou, "Vulnerable plaque: The biomechanics of matter," *Atherosclerosis*, vol. 236, no. 2, pp. 351–352, Oct. 2014.

[15] A. Tuenter, M. Selwaness, A. Arias Lorza, J. C. H. Schuurbiers, L. Speelman, M. Cibis, A. van der Lugt, M. de Bruijne, A. F. W. van der Steen, O. H. Franco, M. W. Vernooij, and J. J. Wentzel, "High shear stress relates to intraplaque haemorrhage in asymptomatic carotid plaques," *Atherosclerosis*, vol. 251, pp. 348–354, Aug. 2016, doi: 10.1016/j.atherosclerosis.2016.05.018.

[16] Y. Qiu and J. M. Tarbell, "Computational simulation of flow in the end-to-end anastomosis of a rigid graft and a compliant artery," *ASAIO J.*, vol. 42, no. 5, pp. M702–M709, Sep. 1996.

[17] Y. Qiu and J. M. Tarbell, "Interaction between wall shear stress and circumferential strain affects endothelial cell biochemical production," *J. Vascular Res.*, vol. 37, no. 3, pp. 147–157, 2000.

[18] D. Tang, C. Yang, J. Zheng, P. K. Woodard, J. E. Saffitz, G. A. Sicard, T. K. Pilgram, and C. Yuan, "Quantifying effects of plaque structure and material properties on stress distributions in human atherosclerotic plaques using 3D FSI models," *J. Biomech. Eng.*, vol. 127, no. 7, pp. 1185–1194, Jan. 2006, doi: 10.1115/1.2073668.

[19] S. Tada and J. M. Tarbell, "A computational study of flow in a compliant carotid bifurcation–stress phase angle correlation with shear stress," *Ann. Biomed. Eng.*, vol. 33, no. 9, pp. 1202–1212, Sep. 2005.

[20] S. Tada, C. Dong, and J. M. Tarbell, "Effect of the stress phase angle on the strain energy density of the endothelial plasma membrane," *Biophys. J.*, vol. 93, no. 9, pp. 3026–3033, Nov. 2007.

[21] R. Torii, N. B. Wood, N. Hadjiloizou, A. W. Dowsey, A. R. Wright, A. D. Hughes, J. Davies, D. P. Francis, J. Mayet, G.-Z. Yang, S. A. M. Thom, and X. Y. Xu, "Stress phase angle depicts differences in coronary artery hemodynamics due to changes in flow and geometry after percutaneous coronary intervention," *Amer. J. Physiol.-Heart Circulatory Physiol.*, vol. 296, no. 3, pp. H765–H776, Mar. 2009.

[22] M. R. Sadeghi, E. Shirani, M. Tafazzoli-Shadpour, and M. Samaee, "The effects of stenosis severity on the hemodynamic parameters—Assessment of the correlation between stress phase angle and wall shear stress," *J. Biomech.*, vol. 44, no. 15, pp. 2614–2626, Oct. 2011.

[23] T. Belzacq, S. Avril, E. Leriche, and A. Delache, "A numerical parametric study of the mechanical action of pulsatile blood flow onto axisymmetric stenosed arteries," *Med. Eng. Phys.*, vol. 34, no. 10, pp. 1483–1495, Dec. 2012.

[24] R. G. Wise, A. I. M. Al-Shafei, T. A. Carpenter, L. D. Hall, and C. L.-H. Huang, "Simultaneous measurement of blood and myocardial velocity in the rat heart by phase contrast MRI using sparseq-space sampling," *J. Magn. Reson. Imag.*, vol. 22, no. 5, pp. 614–627, Nov. 2005.

[25] S. Sampath, J. H. Kim, R. J. Lederman, and E. R. McVeigh, "Simultaneous imaging of myocardial motion and chamber blood flow with SPAMM n' EGGS (spatial modulation of magnetization with encoded gradients for gauging speed)," *J. Magn. Reson. Imag.*, vol. 27, no. 4, pp. 809–817, Apr. 2008.

[26] J. Ge, F. Chirillo, J. Schwedtmann, G. Gorge, M. Haude, D. Baumgart, V. Shah, C. von Birgelen, S. Sack, H. Boudoulas, and R. Erbel, "Screening of ruptured plaques in patients with coronary artery disease by intravascular ultrasound," *Heart*, vol. 81, no. 6, pp. 621–627, Jun. 1999.

[27] M. Yamagishi, M. Terashima, K. Awano, M. Kijima, S. Nakatani, S. Daikoku, K. Ito, Y. Yasumura, and K. Miyatake, "Morphology of vulnerable coronary plaque: Insights from follow-up of patients examined by intravascular ultrasound before an acute coronary syndrome," *J. Amer. College Cardiol.*, vol. 35, no. 1, pp. 106–111, Jan. 2000.

[28] G. S. Mintz, S. E. Nissen, and W. D. Anderson, "American College of Cardiology clinical expert consensus document on standards for acquisition, measurement and reporting of intravascular ultrasound studies (IVUS). A report of the American college of cardiology task force on clinical expert consensus documents developed in collaboration with the European society of cardiology endorsed by the society of cardiac angiography and interventions," *J. Amer. College Cardiol.*, vol. 37, no. 5, pp. 1478–1492, 2001.

[29] B. W. A. M. M. Beulen, N. Bijnens, G. G. Koutsouridis, P. J. Brands, M. C. M. Rutten, and F. N. van de Vosse, "Toward noninvasive blood pressure assessment in arteries by using ultrasound," *Ultrasound Med. Biol.*, vol. 37, no. 5, pp. 788–797, May 2011.

[30] S. Sethuraman, J. H. Amirian, S. H. Litovsky, R. W. Smalling, and S. Y. Emelianov, "Spectroscopic intravascular photoacoustic imaging to differentiate atherosclerotic plaques," *Opt. Express*, vol. 16, no. 5, pp. 3362–3367, Mar. 2008.

[31] F. Rakebrandt, D. C. Crawford, D. Havard, D. Coleman, and J. P. Woodcock, "Relationship between ultrasound texture classification images and histology of atherosclerotic plaque," *Ultrasound Med. Biol.*, vol. 26, no. 9, pp. 1393–1402, Nov. 2000.

[32] M. P. Brewin, P. D. Srodon, S. E. Greenwald, and M. J. Birch, "Carotid atherosclerotic plaque characterisation by measurement of ultrasound sound speed *in vitro* at high frequency, 20 MHz," *Ultrasonics*, vol. 54, no. 2, pp. 428–441, Feb. 2014.

[33] L. Niu, M. Qian, R. Song, L. Meng, X. Liu, and H. A. Zheng, "A 2D non-invasive ultrasonic method for simultaneous measurement of arterial strain and flow pattern," *Clin. Physiol. Funct. Imag.*, vol. 32, no. 4, pp. 323–329, 2012.

[34] M. B. Dancu and J. M. Tarbell, "Large negative stress phase angle (SPA) attenuates nitric oxide production in bovine aortic endothelial cells," *J. Biomech. Eng.*, vol. 128, no. 3, pp. 329–334, Jun. 2006.

[35] H. B. Atabek, S. C. Ling, and D. J. Patel, "Analysis of coronary flow fields in thoracotomized dogs," *Circulat. Res.*, vol. 37, no. 6, pp. 752–761, Dec. 1975.

[36] L. Niu, M. Qian, K. Wan, W. Yu, Q. Jin, T. Ling, S. Gao, and H. Zheng, "Ultrasonic particle image velocimetry for improved flow gradient imaging: Algorithms, methodology and validation," *Phys. Med. Biol.*, vol. 55, no. 7, pp. 2103–2120, Apr. 2010.

[37] D. P. Hart, "PIV error correction," in *Laser Techniques Applied to Fluid Mechanics*. Berlin, Germany: Springer, 2000, pp. 19–35.

[38] D. M. King, C. M. Moran, J. D. McNamara, A. J. Fagan, and J. E. Browne, "Development of a vessel-mimicking material for use in anatomically realistic Doppler flow phantoms," *Ultrasound Med. Biol.*, vol. 37, no. 5, pp. 813–826, May 2011.

[39] J. Fromageau, E. Brusseau, D. Vray, G. Gimenez, and P. Delachartre, "Characterization of PVA cryogel for intravascular ultrasound elasticity imaging," *IEEE Trans. Ultrason., Ferroelectr, Freq. Control*, vol. 50, no. 10, pp. 1318–1324, Oct. 2003.

[40] L. Niu, M. Qian, L. Yan, W. Yu, B. Jiang, Q. Jin, Y. Wang, R. Shandas, X. Liu, and H. Zheng, "Real-time texture analysis for identifying optimum microbubble concentration in 2-D ultrasonic particle image velocimetry," *Ultrasound Med. Biol.*, vol. 37, no. 8, pp. 1280–1291, Aug. 2011.

[41] H. A. Pakravan, M. S. Saidi, and B. Firoozabadi, "A mechanical model for morphological response of endothelial cells under combined wall shear stress and cyclic stretch loadings," *Biomech. Model. Mechanobiol.*, vol. 15, no. 5, pp. 1229–1243, Oct. 2016.

[42] H. Kang, Y. Zhang, X. Huang, L. Niu, H. Zhang, L. Xu, and D. Abbott, "Quantification of atherosclerotic plaque elasticity using ultrasonic texture matching," *IEEE Access*, vol. 8, pp. 94268–94278, 2020, doi: 10.1109/ACCESS.2020.2996432.

LISHENG XU (Senior Member, IEEE) received the B.S. degree in electrical power system automation, the M.S. degree in mechanical electronics, and the Ph.D. degree in computer science and technology from the Harbin Institute of Technology, Harbin, China, in 1998, 2000, and 2006, respectively.

He is currently a Full Professor with the Sino-Dutch Biomedical and Information Engineering School, Northeastern University, China. He has authored or coauthored 139 international research articles and holds 15 invention patents. His current research interests include nonlinear medical signal processing, computational electromagnetic simulation, medical imaging, and pattern recognition. He is a Senior Member of the Chinese Society of Biomedical Engineering. He is a member of the editor board for many international journals such as *Physiological Measurement*, *BioMedical Engineering OnLine*, and *Computers in Biology and Medicine*. He is the Director of the Theory and Education Professional Committee of the China Medical Informatics Association.

YANLING ZHANG received the bachelor's degree in clinical medicine from the Xiangya School of Medicine, Central South University, Changsha, China, in 2004, and the master's degree in imaging and nuclear medicine and the Ph.D. degree in internal medicine from Sun Yat-sen University, Guangzhou, China, in 2007 and 2014, respectively. Since 2007, she has been working with the Department of Ultrasound, Third Affiliated Hospital, Sun Yat-sen University, for more than ten years. She is a Principal Investigator of two projects, including the Chinese National Natural Science Foundation Grant. Her research interest includes the clinical application of new ultrasonic technology, including application of contrast-enhanced ultrasound, ultrasound of liver transplantation, evaluation of vascular wall and plaque by elastography, and early diagnosis of atherosclerosis. She has authored or coauthored more than 30 refereed research articles related to above research fields.

LONG MENG (Member, IEEE) received the B.Sc. degree in electrical and information engineering from the Shenyang University of Technology, China, in 2007, and the Ph.D. degree in pattern recognition and intelligent system from the University of Chinese Academy of Sciences, in 2012. He is currently an Associate Professor with the Shenzhen Institutes of Advanced Technology, Chinese Academy of Sciences (CAS). His research interests include acoustic tweezers, ultrasound bioeffects, and neuro-modulation. He was awarded the Guangdong Natural Science Funds for Distinguished Young Scholar, the Guangdong Youth Talent Support Program, and the Youth Innovation Promotion Association CAS.

SHUAI LI received the B.Eng. and M.Eng. degrees in biomedical engineering from Northeastern University, Shenyang, China, in 2014 and 2017, respectively. He was a Visiting Student with the Shenzhen Institute of Advanced Technology, Shenzhen, China, from 2015 to 2016. He is currently studying with The Hong Kong Polytechnic University, Hong Kong.

LILI NIU (Member, IEEE) received the master's degree in biomedical engineering from Northeastern University, China, in 2009, and the Ph.D. degree in computer application technology from the Chinese Academy of Sciences (CAS), in 2012. She is currently an Associate Professor with the Shenzhen Institute of Advanced Technology, CAS. She has published more than 30 peer-reviewed journals in the biomedical engineering field and applied more than ten patents. She is a Principal Investigator of six projects, including the National Natural Science Foundation Grant of China and so on. Her main research interests include developing advanced biomedical ultrasound techniques for investigating vascular biomechanics and ultrasound neuromodulation.

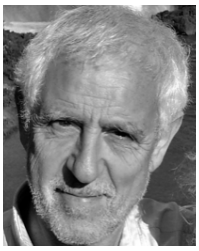

STEPHEN E. GREENWALD received the B.A. degree in natural science from the University of Oxford, in 1970, and the Ph.D. degree in medicine from the University of London, in 1975. He is currently a Professor of cardiovascular mechanics with the Barts and The London School of Medicine and Dentistry, Queen Mary University of London. He holds a Visiting Professorship with the Department of Mathematics, Brunel University London. His research interests include the relationship between structure and function in elastic tissues, mechanical factors in the pathogenesis of cardiovascular disease and the development of non-invasive optical and acoustic methods, for measuring arterial stiffness, endothelial function, and the detection of disturbed flow associated with coronary and carotid artery disease. He is a member of the Institute of Bioengineering, Queen Mary University of London, and the Vice President of the International Society of Pathophysiology.

HUI ZHANG received the master's degree in cardiovascular medicine and the Ph.D. degree in ultrasound medicine from Sun Yat-sen University, Guangzhou, China, in 2004 and 2010, respectively. He has worked as a Clinician in the field of cardiovascular medicine for eight years. He has worked with the Department of Ultrasound, Third Affiliated Hospital, Sun Yat-sen University, for 15 years. He has participated in nine foundation items as a Principal Investigator or a Collaborator, since 2005. His research interests include the application of ultrasonic techniques to the study of cardiovascular disease, early diagnosis of atherosclerosis, and fetal heart's pathophysiology. He has authored or coauthored more than 30 refereed research articles related to above research fields.

LU WANG (Member, IEEE) received the B.Eng. and M.Eng. degrees in computer science from the Harbin Institute of Technology, Harbin, China, in 2003 and 2005, respectively, and the Ph.D. degree in electronic engineering from The University of Hong Kong, Hong Kong, in 2011. She is currently an Associate Professor with the School of Computer Science and Engineering, Northeastern University, Shenyang, China. Her research interests include computer vision, pattern recognition and biomedical signal, and image analysis.